Supporting Information

Porous Carbon Nanosheets Functionalized with Fe_3O_4 Nanoparticles for Capacitive Removal of Heavy Metal Ions from Water

Cuijiao Zhao,[a,b,†] Xinlei Wang,[c,†] Shengbo Zhang,[a,d] Na Sun,[a] Hongjian Zhou,*[,a] Guozhong Wang,[a] Yunxia Zhang,[a] Haimin Zhang,*[,a] and Huijun Zhao[a,e]

[a] Key Laboratory of Materials Physics, Centre for Environmental and Energy Nanomaterials, Anhui Key Laboratory of Nanomaterials and Nanotechnology, CAS Center for Excellence in Nanoscience, Institute of Solid State Physics, Chinese Academy of Sciences, Hefei 230031, China.

[b] Green intelligence environment school, Yangtze Normal University, Chongqing 408100, China

[c] Anhui Zhuocheng Technology LTD, Hefei 231281, China

[d] University of Science and Technology of China, Hefei 230026, China

[e] Centre for Clean Environment and Energy, Griffith University, Gold Coast Campus, QLD 4222, Australia.

[†] These authors contributed equally in this work.

***Corresponding Author**

E-mail: hjzhou@issp.ac.cn (H. Zhou); zhanghm@issp.ac.cn (H. Zhang)

EXPERIMENT SECTION

Materials

Sugarcane bagasse was bought from the nearby sugar refinery in Hefei (Anhui Provience, China). Chloride acid (HCl, 37.5%) and potassium hydroxide (KOH, ≥85%) were supplied by Sinopharm Chemical Reagent Co. Ltd. Iron nitrate ($Fe(NO_3)\cdot 9H_2O$, ≥98.5%), cadmium nitrate ($Cd(NO_3)_2$, ≥99%), lead nitrate ($Pb(NO_3)_2$, ≥99%), cupric nitrate ($Cu(NO_3)_2$, ≥99%), zinc nitrate ($Zn(NO_3)_2$, ≥99%), magnesium nitrate ($Mg(NO_3)_2$, ≥99%), commercial activated carbon (AC, 99%) and 3-aminopropyltriethoxysilane (APTES, 99%) and ethanol (≥99.7%) were purchased from Sinopharm Chemical Reagent Co. Ltd. Deionized water (18.2 MΩ) was used in all experiments.

Characterizations

The morphologies of materials were characterized by Scanning electron microscopy (SEM, SU 8020), Transmission electron microscopy (TEM, JEOL-2010). The structures of the materials were collected on a power by X-ray diffraction (XRD, Philips X'pert PRO) using Ni-filtered monochromatic Cu Kα radiation (λ Kα1=1.5418 Å) at 40 kV and 40 mA. Raman spectra were performed on a Renishaw Micro-Raman Spectroscopy (Renishaw inVia Reflex) using 532 nm laser excitation. The specific surface areas and pore size distributions of materials were measured by an automated gas sorption analyzer (Autosorb-iQ-Cx). The chemical compositions of the materials were analyzed by X-ray photoelectron spectroscopy (XPS, ESCALAB 250) equipped with Al Kα1, 2 monochromatized radiations at 1486.6 eV X-ray source. Thermal gravimetric analysis (TGA) was performed on a TGA Pyris 1 at a heating rate of 5 $^oC\ min^{-1}$at N_2 and air atmosphere, respectively. The Fe element content in the Fe_3O_4/PGCN composite material were determined by inductively coupled plasma atomic emission spectroscopy (ICP-AES,

ICP-6300, Thermo Fisher Scientific) after microwave digestion of the sample. The concentrations of heavy metal ions were measured by the inductively coupled plasma mass spectrum technique (ICP-MS, iCAP Q, Thermo Fisher Scientific). The contact angles were measured using a Kruss DSA 30 Contact angle tester. Zeta potential (NanoPlus, Micromeritics Instrument Corp) was used to analyze the surface charges at various pH conditions.

Electrochemical measurements

The electrochemical performance of electrodes was evaluated by cyclic voltammetry (CV), galvanostatic charge/discharge (GCD) and Electrochemical impedance spectroscopy (EIS) using a CHI 660E electrochemical station (CHI 660E, CH Instrument, Inc., shanghai, China), using a three-electrode conguration consisted of a working electrode, an Ag/AgCl reference electrode and a Pt counter electrode in 1.0 mol L^{-1} NaCl solution. The cyclic voltammetry (CV) measurement was carried out in the potential range of 0~1.0 V and galvanostatic charge/discharge (GCD) measurement was performed in the potential range of -0.2~1 V. The electrochemical impedance spectroscopy (EIS) was measured with an amplitude of 5.0 mV and frequency range from 100 KHz to 0.01 Hz. Specially, the working electrode was obtained by mixing the Fe_3O_4/PGCN material, acetylene black and nafion solution with the mass ratio was 8:1:1. The mixture was cast on the Ni foam and dried at 60 ^oC overnight in oven. Similarly, the PGCN and SBC electrodes were also prepared as the same method. The specific capacitances from GCD curves were calculated based on the following equation:

$$C = I\Delta t / m\Delta V \quad (1)$$

where I is the discharge current density, Δt is the discharge time, m is the mass of the

active material, and ΔV is the discharge voltage difference.

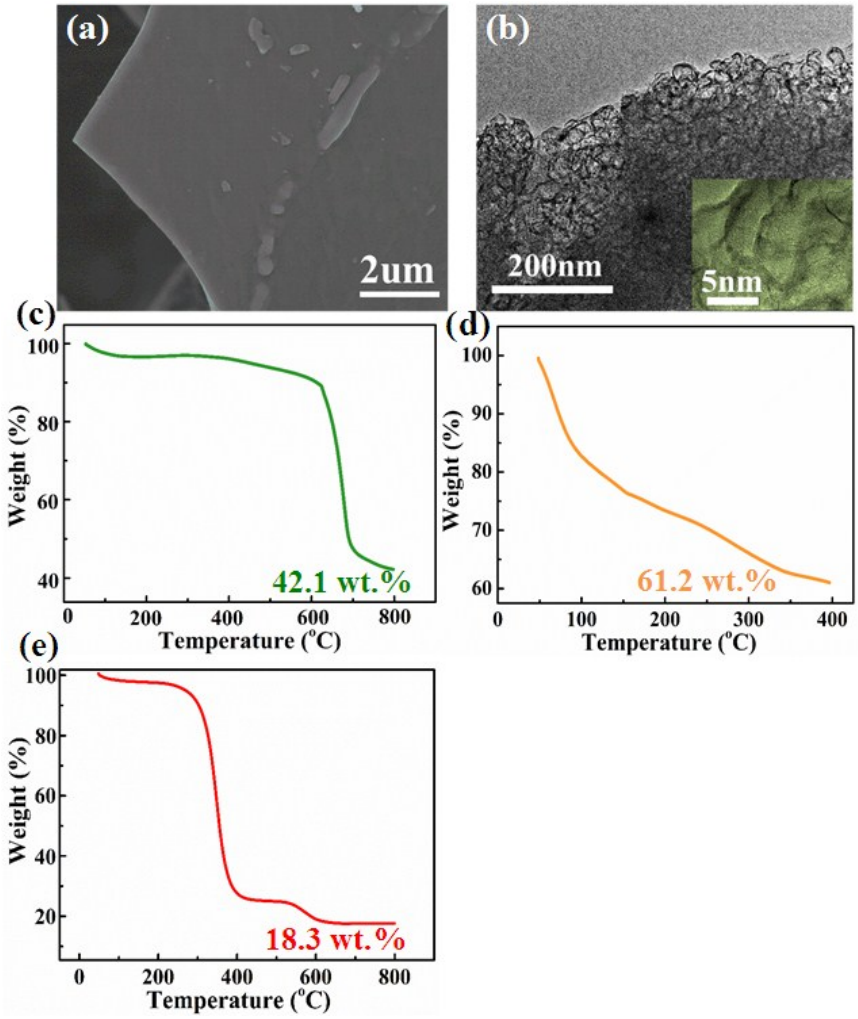

Figure S1. (a) The SEM image of SBC. (b) TEM image of the PGCN (inset shows the enlarged TEM image of PGCN). The TG curves of (c) the mixture of KOH and pre-carbonized sugarcane bagasse in the N_2 atmosphere, (d) the PGCN with $Fe(NO)_3$ in the N_2 atmosphere, (e) the Fe_3O_4/PGCN in the air atmosphere.

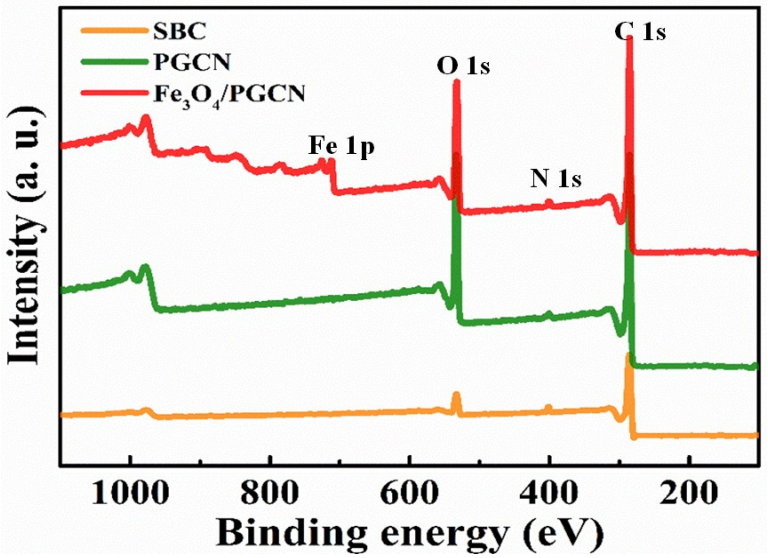

Figure S2. (a) The XPS survey spectra for the SBC, PGCN and Fe_3O_4/PGCN.

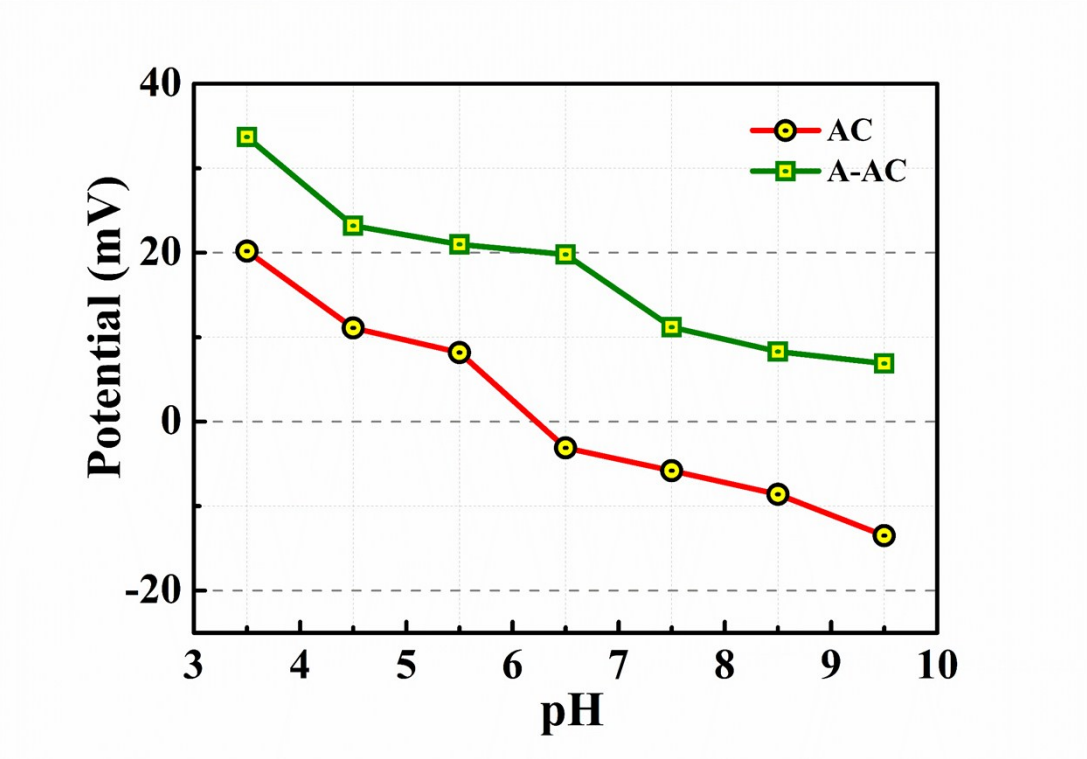

Figure S3. Zeta potential curves of AC and A-AC.

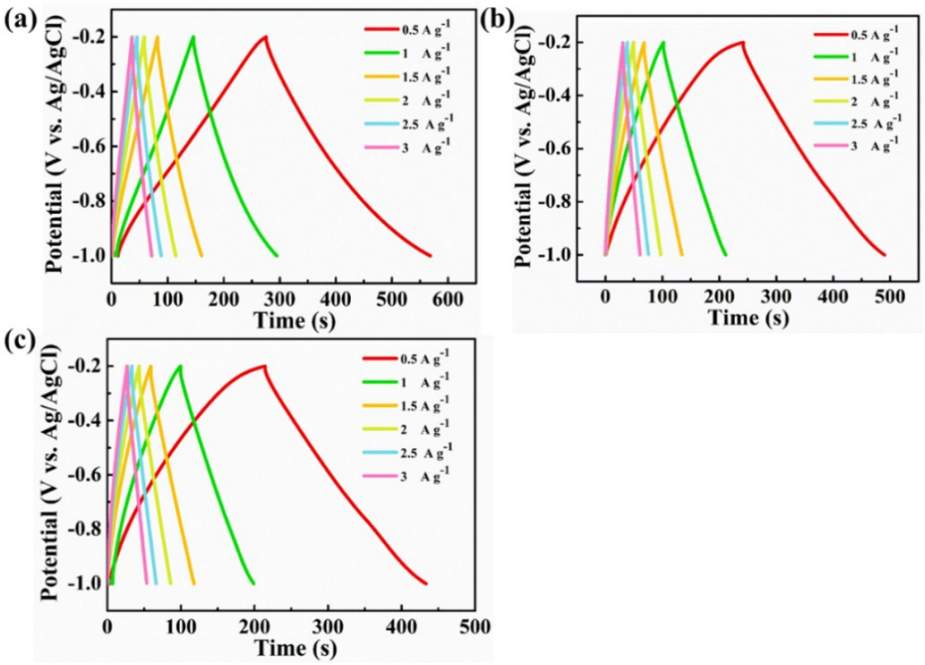

Figure S4. The galvanostatic charge-discharge (GCD) curves of SBC, PGCN and Fe_3O_4/PGCN in 1.0 mol L^{-1} NaCl solution over a potential range from -1.0 to -0.2 V at different current densities.

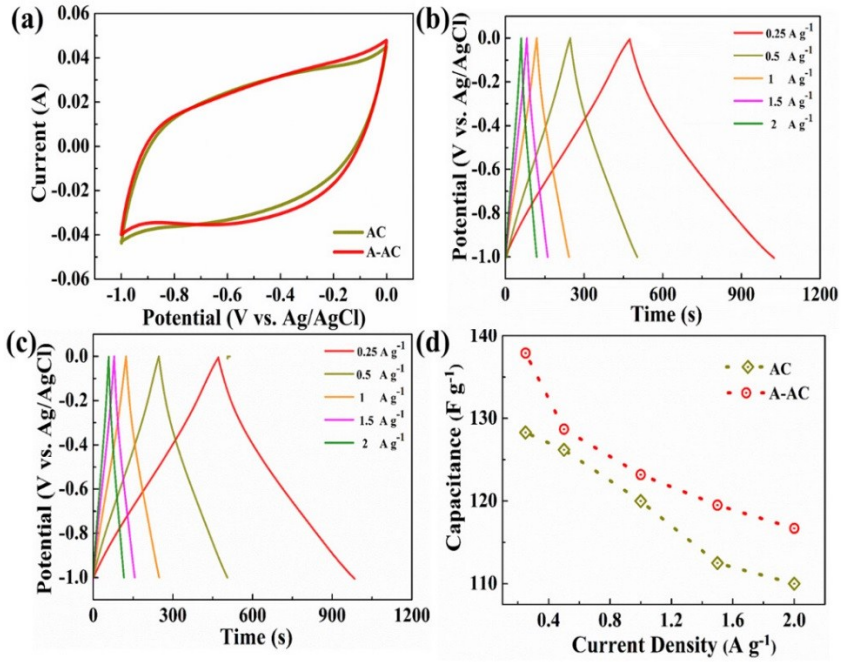

Figure S5. Electrochemical performances of AC and A-AC in 1.0 mol L^{-1} NaCl solution. (a) CV curves of AC and A-AC at scan rate of 100 mV s^{-1}. GCD curves of (b) A-AC, and

(b) AC electrodes over a potential range from -1.0 to 0 V at different current densities. (d) Specific capacitances of AC and A-AC at different current densities.

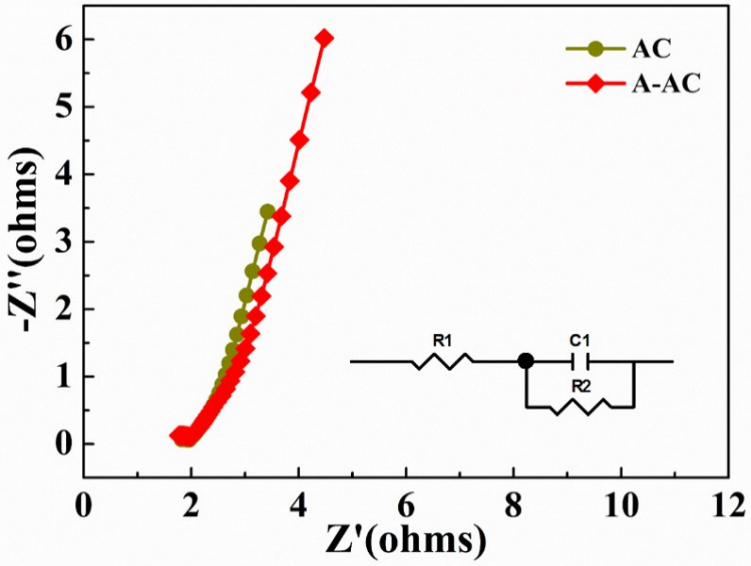

Figure S6. EIS measurements of AC and A-AC electrodes in the test frequency from 0.1 to 10^6 Hz in 1.0 mol L^{-1} NaCl solution. Inset of Figure S9 shows the corresponding equivalent electric circuit.

The cyclic voltammetry (CV) measurements of AC and A-AC were performed. As shown in Figure S5, the integral area of CV curve of A-AC obtained at a scan rate of 100mV s^{-1} in 1.0 mol L^{-1} NaCl solution is larger than that of AC, possibly duo to amino functionalization. Figure S5b-c show the GCD curves of A-AC and AC samples in 1.0 M NaCl solution at different current densities from 0.25 to 2.0 A g^{-1}, and based on these GCD curves, their specific capacitances at different current densities are shown in Figure S5d. A-AC electrode exhibits larger specific capacitances at different current densities compared to AC electrodes. At a current density of 0.25A g^{-1}, the specific capacitance of A-AC can obtain 137.9 F g^{-1}, and the capacitance retentions 84.6% at a current density of 2 A g^{-1}. The EIS of A-AC and AC were measured in 1.0 M NaCl solution, as shown in Figure S6. The Nyquist plots are interpreted with an equivalent circuit, as shown in the

inset of Figure S6 (SI). The R_2 of A-AC and AC are 1.82 and 1.76 respectively. Almost identical series resistance and semicircle radius in high frequency region for AC and A-AC indicate an ignorable influence of amino groups functionalization on the electron transfer of AC.

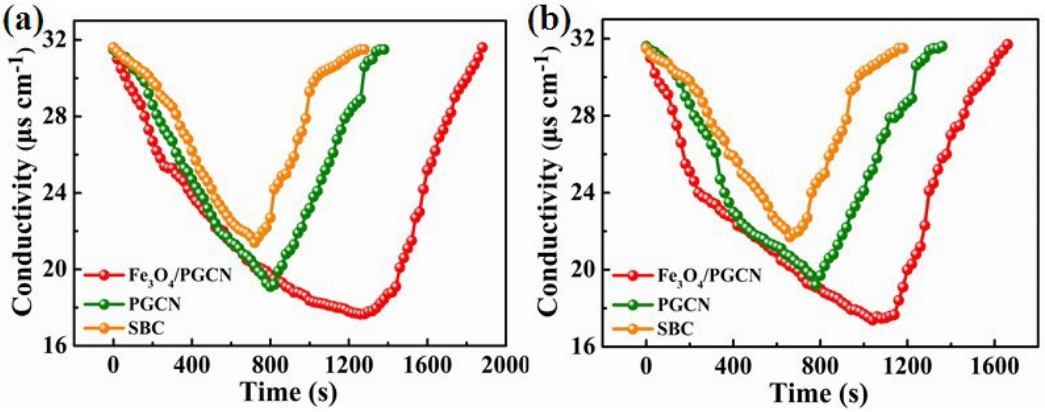

Figure S7. Adsorption and desorption curves of SBC, PGCN and Fe_3O_4/PGCN electrodes at 1.2 V in $Pb(NO_3)_2$ solution (a) and $Cd(NO_3)_2$ solution (b) with an initial concentration of 15 mg L^{-1}.

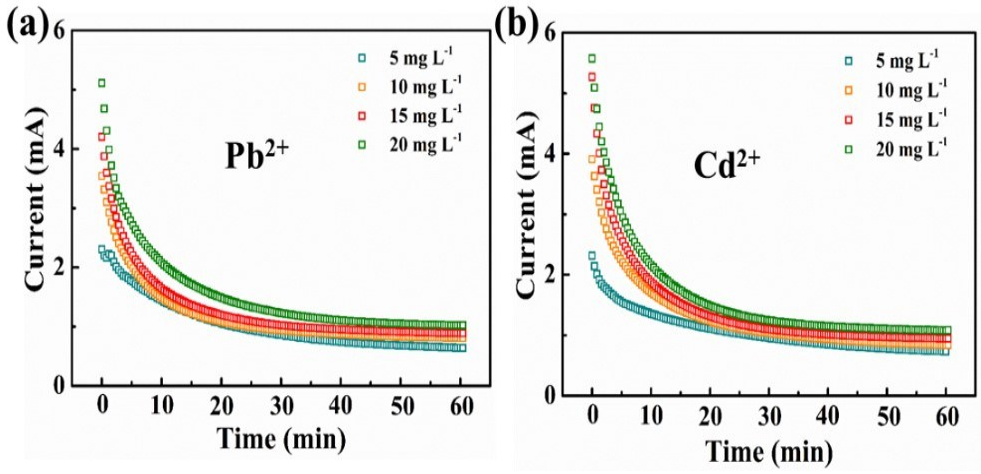

Figure S8. Current transient profiles for the Fe_3O_4/PGCN assembled CDI over 60 min in $Pb(NO_3)_2$ solution (a) and $Cd(NO_3)_2$ solution (b) with different initial concentrations.

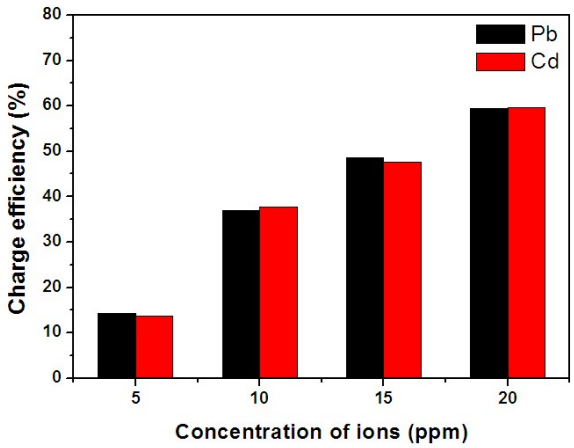

Figure S9. Charge efficiency of the Fe_3O_4/PGCN assembled CDI in $Pb(NO_3)_2$ solution and $Cd(NO_3)_2$ solution with different initial concentrations.

Table S1. Performance comparison of Fe_3O_4/PGCN assembled CDI and most recently reported carbon-based CDI.

Materials	**ions**	**Initial concentration (mg L^{-1})**	**Remove capacity** (mg g-1)	**Removal rate (mg g-1 min-1)**	**Voltage**	**Time**	**References**
Activated carbon cloth(ACC, FM70)	Cd(II)	5.6	1.2 mg/g	0.02	1.2V	120min	1
	Pb(II)	10	6.4 mg/g	0.11			
Porous N-doped graphene nanosheets	Pb(II)	10	36 mg/g	1.6	1.2V	45 min	2
	Cd(II)		32 mg/g	1.4			
Activated carbon	Cu(II)	300	24.6 mg/g	0.2	0.8V	200min	3
3D graphene@EDTA	Pb(II)	20	7 mg/g	0.23	1.4V	60 min	4
Magnetite (Fe_3O_4)/porous graphene nanocomposites	Pb(II)	62	9.3 mg/L	-	1.2 V	-	5
	Cd(II)	34	5.1 mg/L	-			
Fe_3O_4/PGCN	Pb(II)	20	20.9 mg/g	0.7	1.2 V	60 min	**This work**
	Cd(II)	20 mg/L	20.2 mg/L	0.67	1.2 V	60 min	

References

1. Z. Huang, L. Lu, Z. Cai, and Z. J. Ren, Individual and competitive removal of heavy metals using capacitive deionization, *Journal of Hazardous Materials*, 2016**, 302**, 323.

2. L. Liu, X. Guo, R. Tallon, X. Huang, and J. Chen, Highly porous N-doped graphene nanosheets for rapid removal of heavy metals from water by capacitive deionization, *Chemical Communications*, 2017**, 53**, 881.

3. S. Y. Huang, C. S. Fan, and C. H. Hou, Electro-enhanced removal of copper ions from aqueous solutions by capacitive deionization, *Journal of Hazardous Materials*, 2014**, 278**, 8.

4. P. Liu, T. Yan, J. Zhang, L. Shi, and D. Zhang, Separation and recovery of heavy metal ions and salt ions from wastewater by 3D graphene-based asymmetric electrodes via capacitive deionization, *Journal of Materials Chemistry A*, 2017**, 5**, 14748.

5. G. Bharath, E. Alhseinat, N. Ponpandian, M. A. Khan, M. R. Siddiqui, F. Ahmed, and E. H. Alsharaeh, Development of adsorption and electrosorption techniques for removal of organic and inorganic pollutants from wastewater using novel magnetite/porous graphene-based nanocomposites, *Separation and Purification Technology*, 2017**, 188**, 206.